SIGNAL TRANSDUCTION

NF-κB dynamics determine the stimulus specificity of epigenomic reprogramming in macrophages

Quen J. Cheng[1,2]†, Sho Ohta[1]†, Katherine M. Sheu[1], Roberto Spreafico[1,3], Adewunmi Adelaja[1], Brooks Taylor[1], Alexander Hoffmann[1,3]*

The epigenome of macrophages can be reprogrammed by extracellular cues, but the extent to which different stimuli achieve this is unclear. Nuclear factor κB (NF-κB) is a transcription factor that is activated by all pathogen-associated stimuli and can reprogram the epigenome by activating latent enhancers. However, we show that NF-κB does so only in response to a subset of stimuli. This stimulus specificity depends on the temporal dynamics of NF-κB activity, in particular whether it is oscillatory or non-oscillatory. Non-oscillatory NF-κB opens chromatin by sustained disruption of nucleosomal histone–DNA interactions, enabling activation of latent enhancers that modulate expression of immune response genes. Thus, temporal dynamics can determine a transcription factor's capacity to reprogram the epigenome in a stimulus-specific manner.

The cellular epigenome, a regulatory network involving transcription factors, chromatin architecture, and histone modifications, contains stable, heritable information that determines cell type–specific programs of gene expression (*1*, *2*). Nevertheless, the epigenome of differentiated cells remains highly plastic, particularly in immune cells such as macrophages (*3*, *4*). These immune sentinel cells detect microenvironmental immune threats, mount appropriate gene expression responses, and reprogram their epigenomes to tailor subsequent immune responses (*5*). At a molecular level, this reprogramming is initiated by the activity of signal-dependent transcription factors (TFs) such as nuclear factor kappa-light-chain-enhancer of activated B cells (NF-κB) (*6*). In cooperation with chromatin modifiers and pioneering TFs, signal-dependent TFs increase chromatin accessibility and modify histones at previously silent regions of the genome, thus converting latent enhancers to poised or active states (*7*–*9*). NF-κB activated by bacterial lipopolysaccharide (LPS) has been a model TF in this field. However, the degree to which NF-κB or other TFs can alter the epigenome in response to different stimuli is unknown.

To investigate the stimulus specificity of epigenomic reprogramming, we stimulated bone marrow–derived macrophages (BMDMs) with five well-characterized ligands: tumor necrosis factor (TNF) and the Toll-like receptor agonists Pam3CSK, CpG, LPS, and Poly(I:C) (polyinosinic: polycytidylic acid). We performed chromatin immunoprecipitation sequencing (ChIP-seq) using antibodies recognizing the monomethylation of lysine 4 on histone H3 (H3K4me1) to identify latent enhancers that were activated upon stimulation. We found 3978 enhancer regions that segregated into two clusters by the *k*-means algorithm (Fig. 1A and fig. S1). The latent enhancers in cluster 1 were most strongly activated in response to LPS and Poly(I:C) and were enriched for interferon response factor (IRF) motifs (Fig. 1B, top), consistent with the fact that these stimuli activate IRF3 and type I interferon (*10*); in *Irf3*$^{-/-}$*Ifnar*$^{-/-}$ BMDMs, these regions no longer acquired H3K4me1 (Fig. 1C, top). Weak H3K4me1 signal was preserved in response to TNF, which activates IRF1 but not IRF3 (*11*).

In contrast, the regions in cluster 2 were highly enriched for NF-κB motifs (Fig. 1B, bottom), implying that these were latent NF-κB enhancers. We examined the contribution of other stimulus-responsive signaling pathways and found that the gain of H3K4me1 was preserved in *Irf3*$^{-/-}$*Ifnar*$^{-/-}$ BMDMs (Fig. 1C, bottom) but disrupted by pharmacologic inhibition of mitogen-activated protein kinase (MAPK) pathways (fig. S2, A and B). MAPK inhibition also blocked activation of latent enhancers in cluster 1, suggesting that the MAPK pathway is generally critical for epigenomic reprogramming (*12*) and does not specifically collaborate with NF-κB.

We next examined the contribution of NF-κB family members. RelA:p50 is the dominant NF-κB dimer in macrophages (*13*), but cRel also plays a role (*14*). We knocked out cRel (*Rel*$^{-/-}$) and found that H3K4me1 ChIP-seq signals were unchanged (fig. S2C), including at the *Il12b* promoter (*14*). Knocking out p50 (*nfkb1*$^{-/-}$) only weakly diminished H3K4me1 signals, indicating that partial compensation by RelA:p52 or RelA homodimers was sufficient (*15*). These data indicated that RelA is the primary activator of latent NF-κB enhancers in macrophages.

To focus on latent NF-kB enhancers, we used RelA ChIP-seq data (*16*) to identify 1071 regions in cluster 2 that contained a RelA binding event. Unexpectedly, these regions acquired H3K4me1 in a stimulus-specific manner, even though all five stimuli tested activate NF-κB (*17*). Within these regions, the H3K4me1 signal was strongly induced by Pam3CSK, CpG, and LPS, with median $\log_2$ fold changes of 1.07, 1.16, and 1.33, respectively. TNF and Poly(I:C) produced less H3K4me1, with median $\log_2$ fold changes of 0.60 and 0.70, respectively (Fig. 1D, top). A pairwise comparison of samples quantitatively confirmed the stimulus specificity of these NF-κB enhancers (Fig. 1D, bottom).

This stimulus specificity would be difficult to explain if NF-κB acted as a binary on-off switch, but NF-κB is activated with complex, stimulus-specific temporal dynamics (*17*–*19*). In response to various stimuli, NF-κB enters the nucleus with distinct speeds, amplitudes, and durations and may oscillate between the nucleus and cytoplasm. To determine whether stimulus-specific NF-κB dynamics play a role in stimulus-specific activation of latent enhancers, we used live-cell microscopy of BMDMs expressing NF-κB–RelA fused with the mVenus fluorophore (mVenus-RelA) (*20*) to measure the single-cell dynamics of NF-κB–RelA in response to each of the five ligands (Fig. 1E). We quantified the six NF-κB dynamic features that function as signaling codons to encode ligand identity and dose (*20*) and correlated them to mean H3K4me1 counts in the NF-κB–activated latent enhancers (fig. S3). Oscillatory power [correlation coefficient (r) = −0.95], total activity (r = 0.77), and peak amplitude (r = 0.78) were highly correlated with the capacity of a given stimulus to activate latent enhancers (Fig. 1F).

We hypothesized that temporal dynamics of NF-κB activity might affect its interaction with chromatin. Crystallographic studies imply that stable NF-κB–DNA binding requires the DNA to be nucleosome-free, because NF-κB dimers embrace the DNA double helix circumferentially (*21*, *22*) (Fig. 2A). However, NF-κB can interact with nucleosomal DNA, particularly when its binding site is distal to the nucleosome dyad (*23*). Indeed, the DNA-histone interface is composed of low-affinity interactions that allow spontaneous disassociation or "breathing" (*24*). Thus, successive disruptions of DNA-histone contacts by NF-κB, in collaboration with remodeling complexes such as SWI/SNF (*25*), chaperone proteins such as FACT (*26*, *27*), and/or pioneer factors such as Pu.1 or CEB/Pα (*28*), may displace the nucleosome (Fig. 2B). This may be followed by the deposition of histone modifications on neighboring nucleosomes, resulting in a poised or active enhancer (*7*).

We created a multistep model describing how dynamical NF-κB activity might interact

[1]Department of Microbiology, Immunology, and Molecular Genetics, University of California, Los Angeles, CA 90095, USA. [2]Division of Infectious, Diseases Department of Medicine, David Geffen School of Medicine, University of California, Los Angeles, CA 90095, USA. [3]Institute for Quantitative and Computational Biosciences, University of California, Los Angeles, CA 90095, USA.
*Corresponding author. Email: ahoffmann@ucla.edu
†These authors contributed equally to this work.

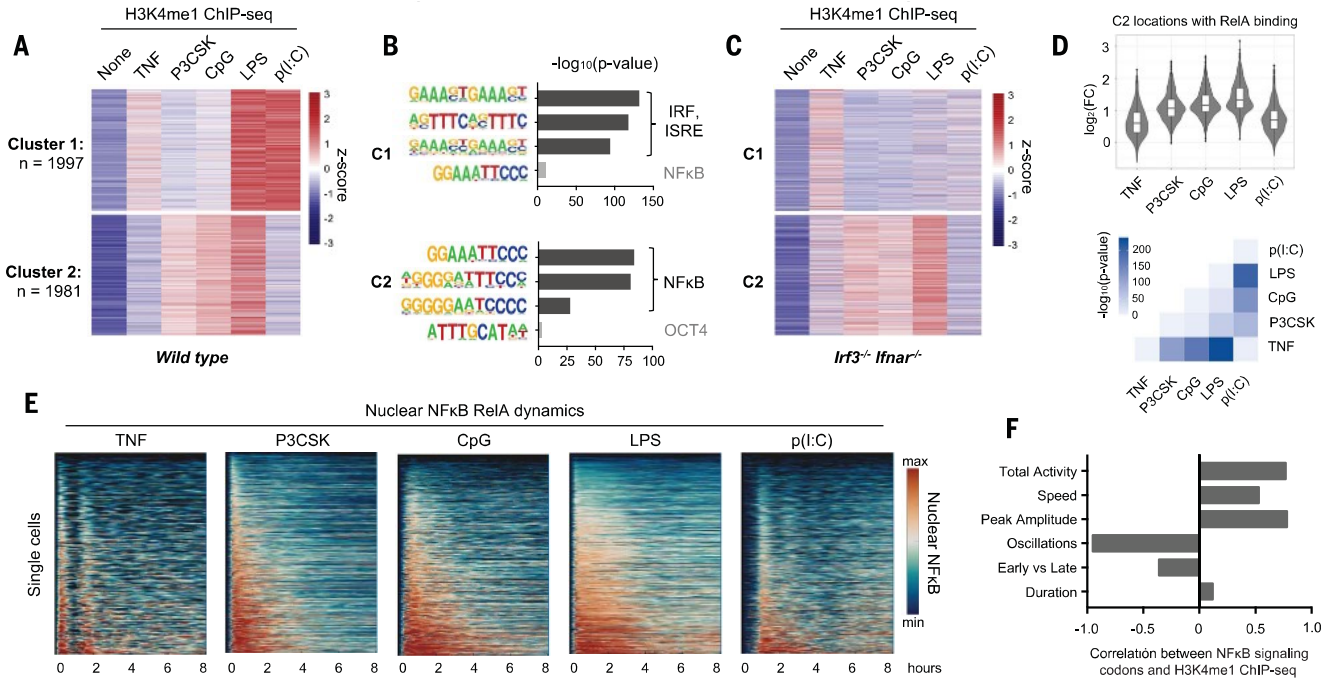

Fig. 1. NF-κB–activated latent enhancers are stimulus-specific and correlate to dynamic features of NF-κB activity. (**A**) Heatmap of H3K4me1 ChIP-seq inducible peaks from BMDMs stimulated with five ligands for 8 hours, unsupervised *k*-means clustering. Average of two biological replicates. (**B**) Known transcription factor motifs with greatest enrichment in cluster 1 and cluster 2 peaks. ISRE, interferon-stimulated response element; OCT4, organic cation/carnitine transporter 4. (**C**) Heatmap of H3K4me1 ChIP-seq in *Irf3*$^{-/-}$*Ifnar*$^{-/-}$ BMDMs, using the same clusters as in (A). (**D**) Violin and box plots of $\log_2$ fold change in H3K4me1 signal of 1071 NF-κB enhancers from cluster 2 that also contain an NF-κB–RelA binding event. Corresponding matrix of *P* values of H3K4me1 ChIP-seq fold change, by two-tailed *t* test between pairs of conditions. (**E**) Heatmaps of NF-κB activity in single cells by live cell microscopy of *mVenus-RelA* BMDMs, showing nuclear abundance of NF-κB in response to five stimuli over 8 hours. (**F**) Bar graph of correlation coefficients between mean H3K4me1 ChIP-seq counts of NF-κB enhancers and the six signaling codons of NF-κB dynamics (*20*); see also fig. S3.

with nucleosomal DNA. A series of 14 Hill equations described the competition between NF-κB and histone for interaction with DNA (Fig. 2C), reflecting the number of contact points in the histone octamer–DNA crystal structure (*29*). Relative rates of nucleosome wrapping and unwrapping were based on available biophysical data (*30*). With measured single-cell NF-κB activities (Fig. 1E) as inputs, the model simulations reproduced the differences in experimental H3K4me1 ChIP-seq data (Fig. 2, D and E, and fig. S4, A and B).

We used the model to investigate which features of NF-κB dynamics affect chromatin accessibility. We examined the three features most highly correlated with the H3K4me1 ChIP-seq data (Fig. 1F): oscillations, amplitude, and total activity. The model indicated that a non-oscillatory dynamic produces a twofold greater chromatin accessibility than an oscillatory dynamic (Fig. 2F). The model also indicated that NF-κB activity must have a minimal amplitude (Fig. 2G and fig. S4C) and extend for a minimal duration (Fig. 2H and fig. S4D) to open chromatin; but above these thresholds, non-oscillatory NF-κB always has greater capacity to open chromatin than does oscillatory NF-κB. This was consistent across a range of parameter values (fig. S5). These simulations predicted that the presence or absence of oscillations, not the maximum amplitude or duration of activity, is the key determinant of whether NF-κB preserves or alters the chromatin state.

To test this prediction, we generated a mouse in which NF-κB dynamics are perturbed. When activated, NF-κB rapidly induces expression of *Nfkbia*, whose gene product is the negative regulator IκBα (Fig. 3A) (*31*). IκBα knockout alone is perinatal lethal owing to persistent inflammation (*32*), but we rescued this lethality by genetically ablating endogenous TNF expression (*33*). We then crossed the composite knockout strain with *mVenus-RelA* knock-in mice to examine the dynamics of NF-κB by live-cell microscopy. IκBα$^{-/-}$ BMDMs responded to TNF with altered NF-κB dynamics compared with wild-type (WT) controls (Fig. 3B). We quantified the differences in the distribution of single-cell dynamic features by the non-parametric Kolmogorov-Smirnov (K-S) test and found that the greatest dynamic difference between IκBα$^{-/-}$ and WT was a loss of oscillations, with a test statistic (*D*) of 0.85, corresponding to $P < 10^{-16}$ (Fig. 3C and fig. S6A). Other dynamic features were either unaffected or favored WT cells, as in the case of activation speed ($D = 0.66$) and early-versus-late activity ($D = 0.52$). The area under the NF-κB activity curve slightly favored WT cells at all time points (Fig. 3C and fig. S6B). We concluded that loss of IκBα abolished NF-κB oscillations without increasing its total activity.

We examined the chromatin state by stimulating BMDMs from IκBα$^{-/-}$ and littermate control mice with TNF and performed the assay for transposase-accessible chromatin using sequencing (ATAC-seq) at 2, 4, and 8 hours. This was followed by a 16-hour period without TNF, after which a final ATAC-seq sample was collected (fig. S7A). We identified 1443 genomic regions that demonstrated TNF-inducible chromatin accessibility in either genotype. Of these, 332 were differentially inducible between control and IκBα$^{-/-}$, and 97% of those 332 regions ($n = 322$) had greater chromatin accessibility in the knockout than in the control (Fig. 3D), despite the slight reduction in total NF-κB activity (fig. S6B). These differentially inducible regions were enriched for NF-κB motifs (Fig. 3E), and 311 of 322 regions showed RelA binding by ChIP-seq (fig. S7B). Ninety-six percent were located in intergenic or intronic portions of the genome (fig. S7C), suggesting that they function as cis-acting enhancers of immune genes such as *Ccl5* (Fig. 3F), which requires chromatin remodeling for maximal expression (*16*).

Our model predicted that chromatin accessibility is primarily determined by whether

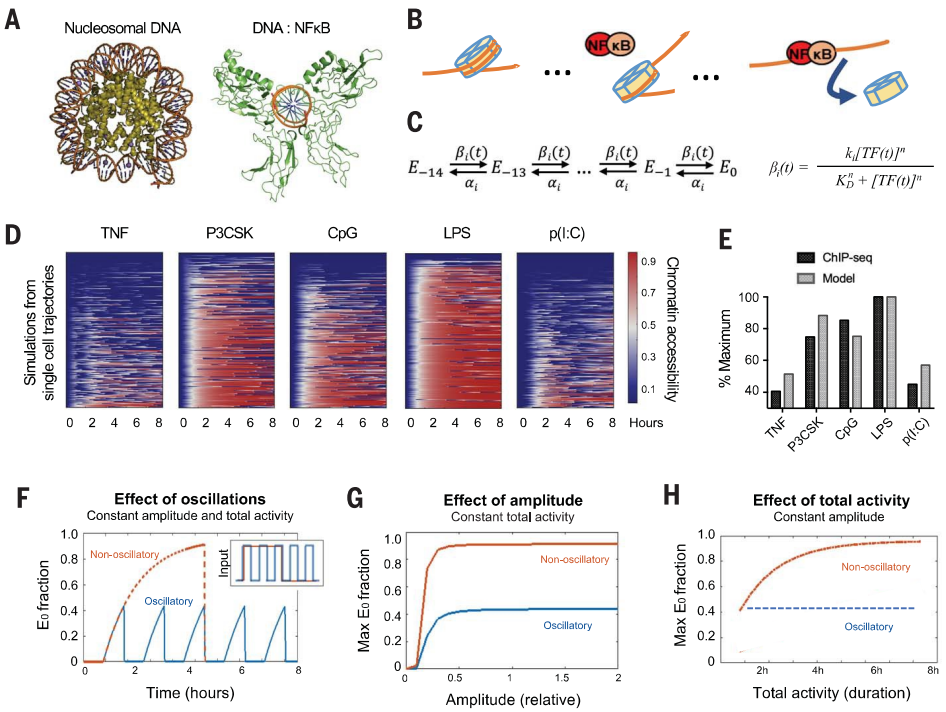

Fig. 2. Mathematical model predicts epigenetic response to distinct dynamic features of NF-κB. (**A**) Crystal structures of nucleosomal DNA [Protein Data Bank (PDB) ID 1F66] versus NF-κB–bound DNA (PDB ID 1VKX), where the RelA:p50 NF-κB dimer is in green. (**B**) Schematic of model illustrating NF-κB–driven nucleosome displacement. (**C**) Multistep model with 14 steps to complete nucleosome unwrapping, each expressed as a Hill function (for further explanation, see supplementary materials). E_{-14}, fully closed state; E_0, fully open state. (**D**) Heatmaps of simulations of chromatin opening in response to different stimuli, using single-cell trajectories from NF-κB microscopy data as input. (**E**) Model simulation versus ChIP-seq data. Mean ChIP-seq counts from 1071 latent NF-κB enhancers (Fig. 1D), background-subtracted and scaled to maximum signal (LPS stimulation). Model simulations are mean of maximum E_0 fraction per cell (compare with fig. S3A), scaled to LPS condition. (**F**) Model simulation of predicted chromatin accessibility comparing oscillatory versus non-oscillatory input activities. (**G** and **H**) Model simulation of predicted chromatin opening across a range of amplitudes and durations.

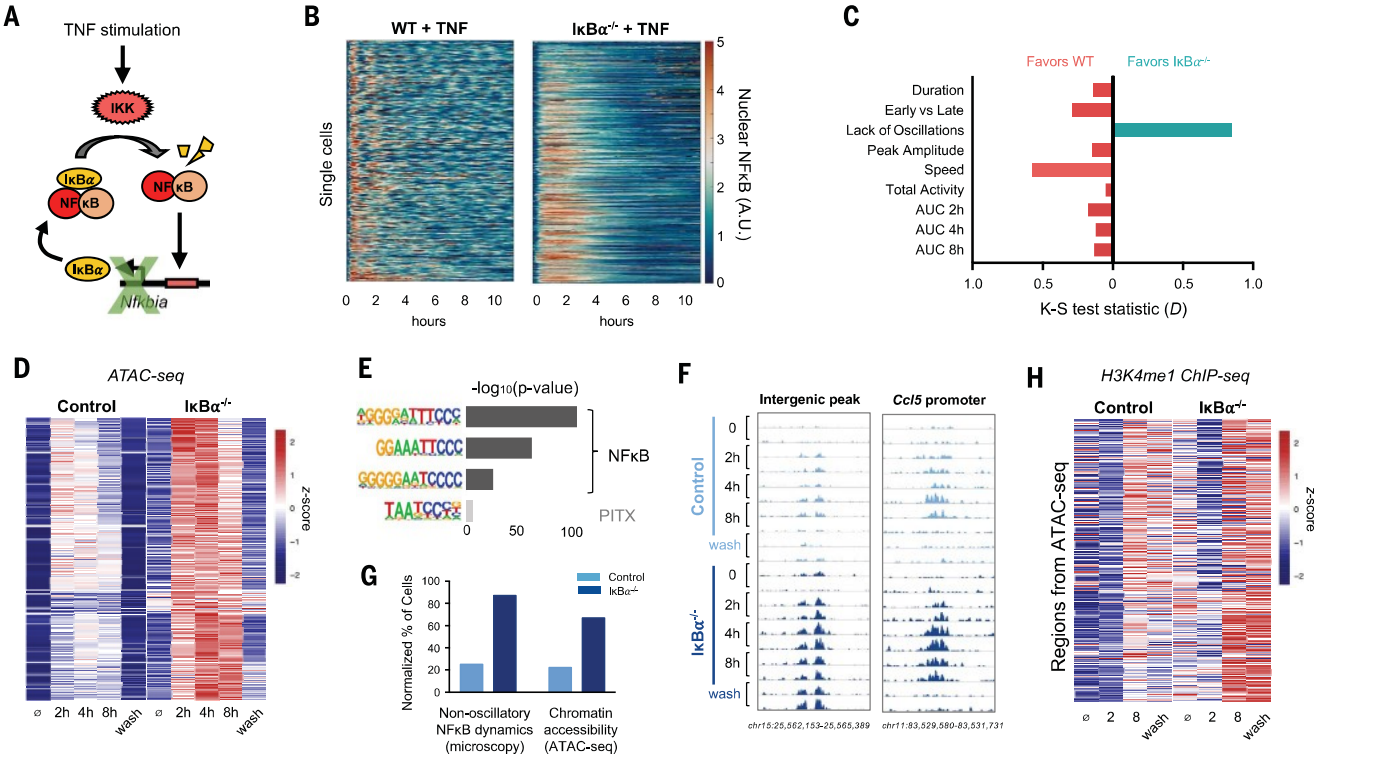

Fig. 3. IκBα knockout abolishes NF-κB oscillations, increases chromatin accessibility, and activates latent enhancers. (**A**) Schematic of IκBα as inducible negative regulator of NF-κB. IKK, IκB kinase. (**B**) Heatmap of single-cell NF-κB activity by live cell microscopy of mVenus-RelA BMDMs, comparing TNF response in WT versus IκBα$^{-/-}$ macrophages. A.U., arbitrary units. (**C**) Bar graph of K-S test statistic for difference in distribution of six signaling codons and areas under NF-κB activity curve (AUC), comparing IκBα$^{-/-}$ and WT. (**D**) Heatmap of ATAC-seq signal after TNF stimulation at 322 genomic regions that are TNF-inducible and differential between IκBα$^{-/-}$ and control. Average of two biological replicates. The term "wash" indicates 8 hours with followed by 16 hours without TNF stimulation. (**E**) Known transcription factor motifs with greatest enrichment in differentially inducible ATAC-seq regions. (**F**) Genome browser tracks for representative differentially inducible ATAC-seq regions, two replicates per time point. (**G**) Percentage of cells with non-oscillatory NF-κB trajectories by microscopy, compared with relative percentage of cells with accessible chromatin by ATAC-seq at *Chr15* intergenic peak (F). (**H**) Heatmap of H3K4me1 ChIP-seq signal after TNF stimulation over the 322 regions defined as differentially inducible by ATAC-seq. Average of two biological replicates. The term "wash" indicates 8 hours with followed by 16 hours without TNF stimulation.

NF-κB is oscillatory or non-oscillatory at the single-cell level. We therefore considered that the magnitude of ATAC-seq signal can be interpreted as the proportion of cells in a sample in which a particular region of DNA is accessible. As determined by microscopy, 87% of IκBα$^{-/-}$ cells had non-oscillatory NF-κB, compared with 25% in WT cells. This was similar to the magnitude of ATAC-seq differences between IκBα$^{-/-}$ and control. For example, at an intergenic peak on chromosome 15, 67% of IκBα$^{-/-}$ cells showed accessible chromatin, compared with 22% of control cells (Fig. 3G).

To confirm that the negative feedback function of IκBα was indeed critical for the observed effects, we used an IκBα$^{κB/κB}$ mutant in which NF-κB binding sites in the promoter of the *Nfkbia* gene are disrupted (*34*) (fig. S8A). In this model, basal IκBα expression is preserved, and the mice live into adulthood without requiring compound suppressor mutations. We found that upon TNF stimulation, IκBα$^{κB/κB}$ BMDMs activated NF-κB in a non-oscillatory manner with minimal disruption of other dynamic features (fig. S8, B to E). ATAC-seq analysis of TNF-stimulated WT versus IκBα$^{κB/κB}$ BMDMs recapitulated our findings in the IκBα$^{-/-}$ system, with 131 genomic regions demonstrating greater gain of chromatin accessibility in the mutant compared with WT (fig. S8F). These regions were enriched for NF-κB motifs, and 90% showed RelA binding by ChIP-seq (fig. S8, G and H). Taken together, the ATAC-seq data from both IκBα$^{-/-}$ and IκBα$^{κB/κB}$ experimental models indicated that loss of NF-κB oscillations results in greater chromatin accessibility at NF-κB binding sites.

We examined whether regions with differentially inducible chromatin accessibility acquired the corresponding histone mark of enhancers. H3K4me1 ChIP-seq in TNF-stimulated BMDMs showed that in the 322 differentially inducible ATAC-seq regions there was also a greater gain of H3K4me1 signal in IκBα$^{-/-}$ than in littermate controls (Fig. 3H). These histone marks persisted for 16 hours after TNF was removed, suggesting that chromatin opening facilitated by NF-κB may be transient but leads to durable H3K4 methylation even after the stimulus is removed, thus activating a latent enhancer and reprogramming the epigenome.

Because histone methylation is more durable and more indicative of enhancer function, we analyzed the H3K4me1 ChIP-seq data independently and identified 2081 regions that acquired more H3K4 methylation in IκBα$^{-/-}$ cells than did controls (Fig. 4A). These differentially induced, dynamics-dependent enhancers persisted after the TNF stimulus was removed, were enriched for NF-κB motifs (Fig. 4B), and showed significant overlap with the set of stimulus-specific NF-κB enhancers identified

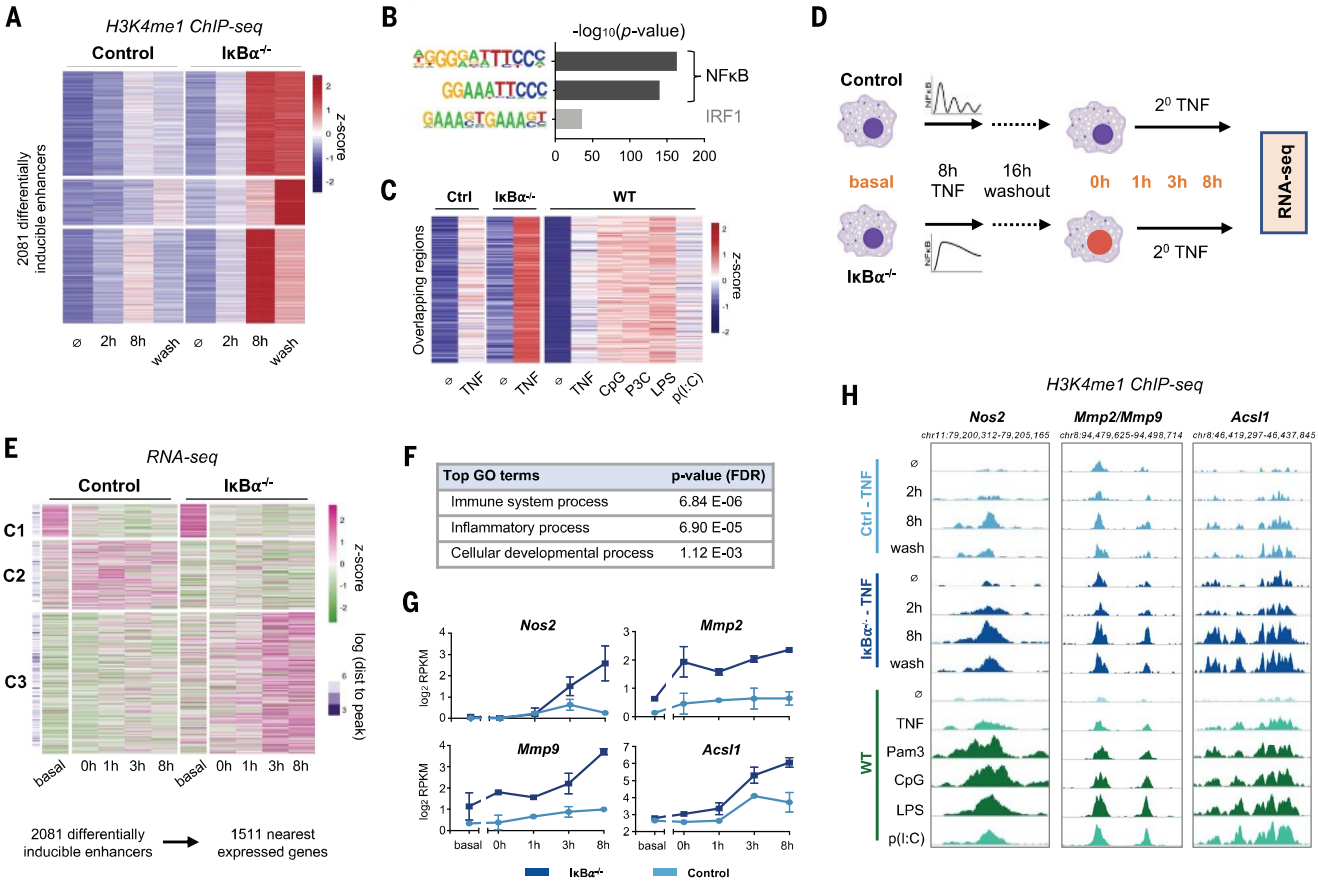

Fig. 4. NF-κB dynamics-dependent enhancers are associated with dynamics-dependent gene expression. (**A**) Heatmap of H3K4me1 ChIP-seq signal after TNF stimulation at 2081 dynamics-dependent enhancers that are differentially induced by TNF between IκBα$^{-/-}$ and control. Average of two biological replicates. The term "wash" indicates 8 hours with followed by 16 hours without TNF. (**B**) Known transcription factor motifs with greatest enrichment in dynamics-dependent enhancers. (**C**) Heatmap of H3K4me1 signal after 8-hour stimulation at regions that overlap between (A) and Fig. 1D (n = 211 regions, P for overlap = 3.0 × 10^{-135}). (**D**) Schematic of RNA-seq experiment. (**E**) Heatmap showing expression of genes closest to dynamics-dependent enhancers, where cluster 3 exhibits differential gene expression between IκBα$^{-/-}$ and control. Average of two biological replicates. (**F**) Top biological process ontology terms for genes in cluster 3 of (E). FDR, false discovery rate. (**G**) Examples of genes differentially induced between IκBα$^{-/-}$ and control, average and standard deviation of two replicates. RPKM, reads per kilobase per million mapped reads. (**H**) Genome browser tracks of differentially inducible H3K4me1 peaks near differentially inducible genes, showing TNF-stimulated IκBα$^{-/-}$ versus control and stimulus-specific response in WT BMDMs. More darkly shaded tracks indicate non-oscillatory NF-κB conditions. Average of two biological replicates.

previously (Fig. 1D, 211 genomic regions, $P = 3.0 \times 10^{-135}$). The inducible ChIP-seq signal was consistently greater when NF-κB dynamics were non-oscillatory rather than oscillatory, whether by genetic perturbation or by stimulus-specific signaling mechanisms (Fig. 4C).

We tested whether NF-κB dynamics-dependent enhancers alter macrophage transcriptional responses to subsequent stimulation. We treated IκBα$^{-/-}$ and littermate control BMDMs with TNF for 8 hours, let cells rest for 16 hours, and then restimulated with TNF for up to 8 hours and collected samples for mRNA sequencing (mRNA-seq) (Fig. 4D). We explored the relation between differentially inducible enhancers and gene expression with two approaches. First, we identified the nearest expressed genes to the 2081 enhancers, removed duplicates, and found three distinct patterns of expression for the resulting 1511 genes (Fig. 4E). Cluster 1 and 2 genes were not TNF-responsive in either condition, reflecting an intrinsic limitation of this approach in which enhancers often do not regulate their nearest genes (*35*). Despite this limitation, cluster 3 genes (58% of total) were both TNF-responsive and more strongly induced in IκBα$^{-/-}$ BMDMs. Of these genes, 88% were not induced in controls at all (using a twofold threshold). These differentially regulated genes were enriched for ontology terms "immune system process" and "inflammatory process" (Fig. 4F), indicating that non-oscillatory NF-κB epigenetically reprograms macrophages to enhance their immune response.

We also examined our data with a gene-centric approach. From the RNA-seq dataset, we identified 1958 TNF-inducible genes, 482 of which were differentially induced in IκBα$^{-/-}$ versus control (fig. S9, A and B). For each gene, we annotated the genomic distance to the nearest differentially inducible H3K4me1 ChIP-seq peak. Differentially induced genes were closer to differentially induced ChIP-seq peaks ($P = 1.13 \times 10^{-9}$) than genes that were not differentially induced (fig. S9, C and D). Thus, both analyses indicated that NF-κB dynamics-dependent enhancers regulate gene expression responses to a subsequent stimulus.

The dynamics-dependent gene expression program included *Nos2*, *Mmp2*, and *Mmp9*, which are well-defined markers of classical macrophage activation (*36*), as well as *Acsl1*, which plays a role in the pathogenesis of atherosclerosis (*37*) (Fig. 4G). Each of these genes had a nearby enhancer that acquired more H3K4me1 signal in the presence of non-oscillatory NF-κB, whether in the IκBα$^{-/-}$ system or in WT BMDMs stimulated with various ligands (Fig. 4H). These specific examples further suggested that latent enhancers activated by non-oscillatory NF-κB regulate genes involved in macrophage activation.

Our results indicate that the dynamics of NF-κB activity, particularly whether it is oscillatory or non-oscillatory, determine NF-κB's capacity to reprogram the macrophage epigenome. We show with a mathematical model how biophysical principles governing nucleosome dynamics might decode stimulus-specific NF-κB dynamical features. The role of temporal dynamics may thus complement the structure-function model in which distance from the nucleosome core determines accessibility to partially exposed DNA motifs (*38*). Together, TF dynamics and motif accessibility may regulate the sensitivity of a particular nucleosome to eviction. To date, the function of NF-κB oscillations has been unclear given that there is little difference in the expression of poised inflammatory-response genes induced by oscillatory versus non-oscillatory NF-κB (*39*, *40*). We propose that in response to some stimuli, the role of oscillations is to maintain the epigenomic state while exploiting existing poised enhancers for inflammatory gene activation. However, in response to other immune threats, non-oscillatory NF-κB induces a comparable gene expression program while also activating latent enhancers, thus changing the epigenomic state of the cell and its response to subsequent stimuli. Although further work will be needed to determine the physiological implications of NF-κB dynamics-dependent enhancers and to identify the proteins that collaborate with NF-κB to evict nucleosomes, our study establishes TF temporal dynamics as a key mechanistic determinant of epigenomic reprogramming.

REFERENCES AND NOTES

1. S. Heinz *et al.*, *Mol. Cell* **38**, 576–589 (2010).
2. C. D. Allis, T. Jenuwein, *Nat. Rev. Genet.* **17**, 487–500 (2016).
3. C. K. Glass, G. Natoli, *Nat. Immunol.* **17**, 26–33 (2016).
4. L. B. Ivashkiv, *Trends Immunol.* **34**, 216–223 (2013).
5. P. J. Murray, T. A. Wynn, *Nat. Rev. Immunol.* **11**, 723–737 (2011).
6. T. Lawrence, *Cold Spring Harb. Perspect. Biol.* **1**, a001651 (2009).
7. R. Ostuni *et al.*, *Cell* **152**, 157–171 (2013).
8. M. U. Kaikkonen *et al.*, *Mol. Cell* **51**, 310–325 (2013).
9. S. Heinz, C. E. Romanoski, C. Benner, C. K. Glass, *Nat. Rev. Mol. Cell Biol.* **16**, 144–154 (2015).
10. K. Honda, A. Takaoka, T. Taniguchi, *Immunity* **25**, 349–360 (2006).
11. A. Yarilina, K.-H. Park-Min, T. Antoniv, X. Hu, L. B. Ivashkiv, *Nat. Immunol.* **9**, 378–387 (2008).
12. A. M. Klein, E. Zaganjor, M. H. Cobb, *Curr. Opin. Cell Biol.* **25**, 272–277 (2013).
13. S. Mitchell, J. Vargas, A. Hoffmann, *Wiley Interdiscip. Rev. Syst. Biol. Med.* **8**, 227–241 (2016).
14. S. Sanjabi, A. Hoffmann, H.-C. Liou, D. Baltimore, S. T. Smale, *Proc. Natl. Acad. Sci. U.S.A.* **97**, 12705–12710 (2000).
15. A. Hoffmann, T. H. Leung, D. Baltimore, *EMBO J.* **22**, 5530–5539 (2003).
16. A.-J. Tong *et al.*, *Cell* **165**, 165–179 (2016).
17. S. L. Werner, D. Barken, A. Hoffmann, *Science* **309**, 1857–1861 (2005).
18. M. Behar, A. Hoffmann, *Curr. Opin. Genet. Dev.* **20**, 684–693 (2010).
19. M. W. Covert, T. H. Leung, J. E. Gaston, D. Baltimore, *Science* **309**, 1854–1857 (2005).
20. A. Adelaja *et al.*, *Immunity* **54**, 916–930.e7 (2021).
21. F. E. Chen, D. B. Huang, Y. Q. Chen, G. Ghosh, *Nature* **391**, 410–413 (1998).
22. R. K. Suto, M. J. Clarkson, D. J. Tremethick, K. Luger, *Nat. Struct. Biol.* **7**, 1121–1124 (2000).
23. I. N. Lone *et al.*, *PLOS Genet.* **9**, e1003830 (2013).
24. G. Li, M. Levitus, C. Bustamante, J. Widom, *Nat. Struct. Mol. Biol.* **12**, 46–53 (2005).
25. K. Kobayashi *et al.*, *Sci. Rep.* **7**, 11772 (2017).
26. A. V. Gasparian *et al.*, *Sci. Transl. Med.* **3**, 95ra74 (2011).
27. D. D. Winkler, K. Luger, *J. Biol. Chem.* **286**, 18369–18374 (2011).
28. F. Jin, Y. Li, B. Ren, R. Natarajan, *Proc. Natl. Acad. Sci. U.S.A.* **108**, 5290–5295 (2011).
29. C. A. Davey, D. F. Sargent, K. Luger, A. W. Maeder, T. J. Richmond, *J. Mol. Biol.* **319**, 1097–1113 (2002).
30. H. S. Tims, K. Gurunathan, M. Levitus, J. Widom, *J. Mol. Biol.* **411**, 430–448 (2011).
31. A. Hoffmann, A. Levchenko, M. L. Scott, D. Baltimore, *Science* **298**, 1241–1245 (2002).
32. A. A. Beg, W. C. Sha, R. T. Bronson, D. Baltimore, *Genes Dev.* **9**, 2736–2746 (1995).
33. V. F.-S. Shih *et al.*, *Proc. Natl. Acad. Sci. U.S.A.* **106**, 9619–9624 (2009).
34. B. Peng *et al.*, *Proc. Natl. Acad. Sci. U.S.A.* **107**, 15193–15198 (2010).
35. M. R. Corces *et al.*, *Science* **362**, eaav1898 (2018).
36. P. J. Murray *et al.*, *Immunity* **41**, 14–20 (2014).
37. J. E. Kanter *et al.*, *Proc. Natl. Acad. Sci. U.S.A.* **109**, E715–E724 (2012).
38. A. Soufi *et al.*, *Cell* **161**, 555–568 (2015).
39. D. Barken *et al.*, *Science* **308**, 52 (2005).
40. C. S. Cheng *et al.*, *Cell Syst.* **4**, 330–343.e5 (2017).
41. Signaling Systems Lab, signalingsystemslab/NFkB_enhancer_dynamics: First release bioinfo analysis and nucleosome model, Version 1.0, Zenodo (2021); http://doi.org/10.5281/zenodo.4698447.

ACKNOWLEDGMENTS

We thank K. Kishimoto, D. Lefaudeux, X.-F. Lin, and A. Mazumber for their experimental and analytical contributions, and S. Kurdistani, M. Carey, E. Lin, and Y. Tang for their insights and critical reading of the manuscript. **Funding:** This work was supported by NIH grants R01-AI127864 (to A.H.), R01-GM117134 (to A.H.), F31-AI138450 (to A.A.), T32-GM008042 (to K.M.S.), T32-HL069766 (to A.A.), and T32-AI089398 (to Q.J.C.); the Specialty Training and Advanced Research (STAR) program of the UCLA Department of Medicine (to Q.J.C.); and the QCB Collaboratory for a postdoctoral fellowship (to R.S.). Sequencing was performed at the UCLA Broad Stem Cell Center Sequencing Core. **Author contributions:** Q.J.C., S.O., A.A., and B.T. performed the experiments. Q.J.C., S.O., K.M.S., R.S., and A.A. analyzed the data. K.S. and B.T. developed the mathematical model. Q.J.C., K.M.S., and A.H. wrote the manuscript. All authors reviewed the manuscript. A.H. coordinated and funded the work. **Competing interests:** The authors declare no competing interests. **Data and materials availability:** Raw data and count tables for ChIP-seq, ATAC-seq, and RNA-seq data have been submitted to the NCBI GEO repository under accession number GSE146068. Code is available at https://github.com/signalingsystemslab/NFkB_enhancer_dynamics and Zenodo (*41*).

SUPPLEMENTARY MATERIALS

science.sciencemag.org/content/372/6548/1349/suppl/DC1
Materials and Methods
Figs. S1 to S9
References (*42*–*60*)
MDAR Reproducibility Checklist

View/request a protocol for this paper from *Bio-protocol*.

1 April 2020; accepted 22 April 2021
10.1126/science.abc0269

NF-κB dynamics determine the stimulus specificity of epigenomic reprogramming in macrophages

Quen J. Cheng, Sho Ohta, Katherine M. Sheu, Roberto Spreafico, Adewunmi Adelaja, Brooks Taylor and Alexander Hoffmann

Science **372** (6548), 1349-1353.
DOI: 10.1126/science.abc0269

Timing cues epigenomic reprogramming

Different temporal dynamics of activation of the transcription factor nuclear factor κB (NF-κB) can influence the inflammatory response of activated macrophages. Cheng *et al.* report a mechanism by which oscillatory and sustained NF- κB signaling may produce distinct transcriptional responses (see the Perspective by Nandagopal *et al.*). Oscillatory activation of NF- κB activated poised enhancers to transcribe inflammatory genes in mouse macrophages. However, sustained activation of NF- κB produced in cells activated by other stimuli acted on the epigenome. These stimuli relieved chromatin silencing at enhancers and enabled regulation of additional genes.

Science, abc0269, this issue p. 1349; see also abj2040, p. 1263

Science (print ISSN 0036-8075; online ISSN 1095-9203) is published by the American Association for the Advancement of Science, 1200 New York Avenue NW, Washington, DC 20005. The title *Science* is a registered trademark of AAAS.